Cyclometallated Pt(II) Complexes Containing a Functionalized Bis-Urea Alkynyl Ligand: Probing Aggregation Mediated by Hydrogen Bonds versus Pt...Pt and pi-pi Interactions

Gaëtan Basuyaux, Anissa Amar, Claire Troufflard, Abdou Boucekkine, Rémi Métivier, Matthieu Raynal, Jamal Moussa, Laurent Bouteiller, Hani Amouri

▶ **To cite this version:**

Gaëtan Basuyaux, Anissa Amar, Claire Troufflard, Abdou Boucekkine, Rémi Métivier, et al.. Cyclometallated Pt(II) Complexes Containing a Functionalized Bis-Urea Alkynyl Ligand: Probing Aggregation Mediated by Hydrogen Bonds versus Pt...Pt and pi-pi Interactions. European Journal of Inorganic Chemistry, 2021, 2021 (35), pp.3622-3631. 10.1002/ejic.202100499 . hal-03331385

HAL Id: hal-03331385
https://hal.science/hal-03331385

Submitted on 16 Sep 2021

HAL is a multi-disciplinary open access archive for the deposit and dissemination of scientific research documents, whether they are published or not. The documents may come from teaching and research institutions in France or abroad, or from public or private research centers.

L'archive ouverte pluridisciplinaire **HAL**, est destinée au dépôt et à la diffusion de documents scientifiques de niveau recherche, publiés ou non, émanant des établissements d'enseignement et de recherche français ou étrangers, des laboratoires publics ou privés.

Cyclometallated Pt(II) Complexes Containing a Functionalized Bis-Urea Alkynyl Ligand: Probing Aggregation Mediated by Hydrogen Bonds *versus* Pt···Pt and π-π Interactions

Gaëtan Basuyaux,[a] Anissa Amar,[b] Claire Troufflard,[a] Abdou Boucekkine,[c] Rémi Métivier,[d] Matthieu Raynal,[a]* Jamal Moussa,[a] Laurent Bouteiller,[a] and Hani Amouri[a]*

[a] Dr. G. Basuyaux, C. Troufflard, Dr. M. Raynal, Dr. L. Bouteiller, Dr. H. Amouri
Sorbonne Université, CNRS,
Institut Parisien de Chimie Moléculaire,
4 place Jussieu, 75005 Paris (France)
e-mail: matthieu.raynal@sorbonne-universite.fr, hani.amouri@sorbonne-universite.fr

[b] Dr. A. Amar
Laboratoire de Chimie et de Physique Quantiques, Faculté des Sciences, U.M.M.T.O,
15000 Tizi-Ouzou (Algeria)

[c] Pr. Em. A. Boucekkine
Univ. Rennes, ISCR UMR 6226 CNRS,
Campus de Beaulieu, 35042 Rennes Cedex (France)

[d] Dr. R. Métivier
PPSM, ENS Cachan, CNRS,
Université Paris-Saclay, 94235 Cachan (France)

Supporting information for this article is given via a link at the end of the document. It includes Figures S1-S9, Tables S1-S2, NMR spectra of compounds, and detailed computational results.

Abstract: Neutral cyclometallated Pt(II) complexes [(C^N$^{t\text{-Bu}}^{N}^{t\text{-Bu}}$)Pt-R] (**4−5**) containing a bis-urea alkynyl (R) ligand have been prepared and fully characterized. The dichotomous nature of **4−5** makes it difficult to anticipate which interactions (hydrogen bonds, π–π stacking and Pt···Pt) will dominate their assembly process. The aggregation properties of **4−5** were thus probed by multifarious analytical (UV/Vis, FT-IR, NMR, MS, CD, emission) and computational (DFT, TD-DFT) techniques. CD analyses of sergeants-and-soldiers type mixtures between **4** and an enantiopure Pt-free monomer **(*S*,*S*)-3** reveal that no amplification of supramolecular helicity occurs in this system. In fact, complex **4** acts as competitor or chain capper, likely through hydrogen bonding, of the homochiral assemblies formed by **(*S*,*S*)-3**. In DMSO, ^{1}H NMR and DOSY analyses indicate that **4** and **5** form aggregates. Likewise, the aggregation is promoted by the addition of H_2O as suggested by red shift of the lowest energy emission band, which might originate from a ^{3}MMLCT excited state. TD-DFT calculations confirm that self-aggregation occurs through Pt···Pt and π-π interactions yielding head-to-tail aggregates in DMSO and DMSO/H_2O mixtures. Our study therefore suggests a (condition dependent) competitive rather than a cooperative mode of action of the different types of interactions present in aggregates of **4−5**.

Introduction

Square-planar platinum complexes with d^8 configuration have received considerable attention due to their peculiar photophysical and spectroscopic properties.[1-2] Such compounds are stable and promote metal−metal, and π–π interactions, that profoundly impact the properties of the electronic excited states.[3-8] Mononuclear platinum(II) complexes with (N^N^N),[3, 5, 9-16] (N^C^N)[2, 8, 17-19] and (C^N^N)[6, 20-29] pincer-type ligands were prepared and their luminescent properties have been tuned by modifying the nature and the electronic properties of the coordinating tridentate unit and the co-ligand as well.[17-18, 25-26] Moreover, the ability of these platinum chromophores to display metal−metal interactions offers an additional strategy to construct supramolecular assemblies and control their formation in presence of external stimuli in solution state.[16] Furthermore they bring dramatic changes in the spectroscopic properties of the ensemble in solution, which make them versatile reporters of structural transitions[16, 30] or of interactions with chemical agents.[31] Additional weak interactions, *e.g.* hydrogen bonds, could further promote the aggregation properties of Pt(II) complexes at the condition that a convenient balance takes place between these interactions within the nanostructure.[13] Recent work has been devoted towards the construction of supramolecular assemblies of molecular Pt[32-40] or other metal[41-44] complexes and hydrogen-bonding moieties. Yam and co-workers reported that a L-glutamine-derived dialkynylplatinum(II) bipyridine complex aggregated through a combination of hydrogen bonding, π−π stacking and Pt···Pt interactions leading to the formation of a metallogel.[36] In contrast, other neutral Pt(II) complexes featuring amide groups were shown to aggregate into one-dimensional (1D) assemblies mostly through hydrogen bonding interactions,[33-34, 37] the directionality of which likely prevented the stacking of the Pt(II) centres. For platinum complexes embedding both aromatic ligands and hydrogen bonding moieties, it thus remains difficult to anticipate which interactions will dominate the assembly process.

In a previous study, we showed that phosphine gold(I) complexes **1-2** connected to a bis-urea based acetylide ligand form one-dimensional (1D) hydrogen-bonded assemblies in solution (Fig. 1).[45] Remarkably, mixing **1-2** and (***S***,***S***)-**3** monomers generates chiral co-assemblies in which the gold(I) aryl acetylide fragment, although adopting an intrinsically achiral linear geometry, is located in a chiral environment as demonstrated by an induced circular dichroism (ICD) signal. This ICD signal is reversed in presence of (***R***,***R***)-**3** and tuned by

ACCEPTED MANUSCRIPT

the relative proportion of the components and the temperature.[45]

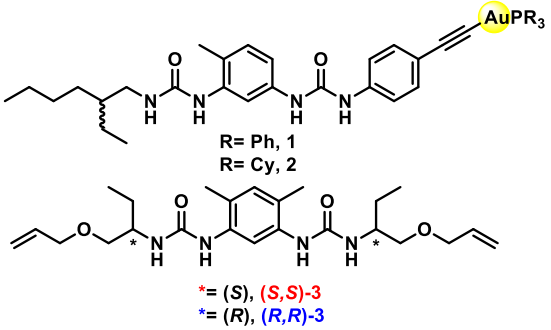

Figure 1 Structure of the $AuPR_3$ acetylide urea complexes **1**-**2** and enantiopure molecules **(*S*,*S*)-3** and **(*R*,*R*)-3** used as monomers of 1D hydrogen-bonded assemblies in our previous studies.[45]

These interesting results prompted us to extend our studies to other metal chromophores displaying different coordination geometries such as square-planar platinum compounds. We expect that combining a neutral Pt(II) centre and a bis-urea unit within the same molecule might allow Pt···Pt, π–π stacking and hydrogen bonding interactions to contribute to the formation of assemblies in organic solvents. Herein, we describe the synthesis of two novel cyclometallated platinum complexes containing bis-urea based alkynyl ligands. To our knowledge, these are the only known examples where a cyclometallated Pt(C^N^N) unit is attached to a bis-urea functionality. Aggregation in solution, solid and gas phases of these Pt complexes, alone or in presence of **(*S*,*S*)-3**, was probed by FT-IR, NMR, mass spectrometry and CD analyses as well as by electronic absorption and emission spectroscopy. These analyses, as well as DFT and TD-DFT calculations, support the competitive rather than cooperative nature of the non-covalent interactions during aggregation of these functionalized Pt complexes.

Results and Discussion

Synthesis, characterization and solubility of cyclometallated complexes 4 and 5

Our target molecules share the following structural elements: 1) a central bis-urea unit with well-established aggregation properties,[46] and 2) a peripheral Pt complex bearing a (C^N^$^{t\text{-}Bu}$^N^$^{t\text{-}Bu}$) pincer-type ligand. Such a neutral cyclometallated Pt moiety was selected for both its stability and its compatibility with hydrogen-bonded moieties. Cyclometallated complexes **4** and **5** were prepared upon reaction of their respective bis-urea aryl acetylene precursors **EHUTE** and ***i*PentUXE** with [PtCl(C^N^$^{t\text{-}Bu}$^N^$^{t\text{-}Bu}$)][47] in MeOH in presence of Cs_2CO_3 and were isolated in satisfactory yields, *ca.* 70% (Scheme 1). NMR and High Resolution Mass Spectroscopy analyses corroborate the expected molecular structures (Supporting Information). The bis-urea acetylide ligand in **5** differs from that of **4** and of our previously designed urea complexes[45] by the presence of an additional methyl group on the aromatic spacer between the urea units and by a shorter branched side chain (isopentyl *versus* 2-ethylhexyl). The first modification was made to foster stronger hydrogen bonds between the urea units,[48-50] and the second to check a potential impact of the

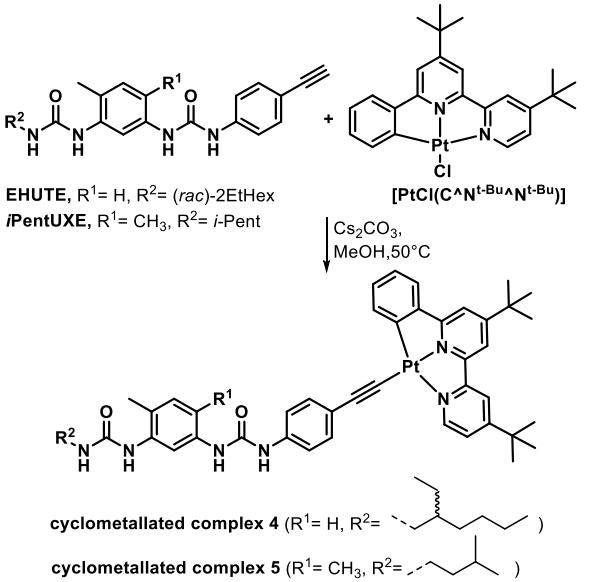

Scheme 1 Synthetic scheme for the preparation of the cyclometallated complexes **4** and **5**.

stereogenic centre on the assembly properties (**4** and **5** are chiral racemic and achiral monomers, respectively). Compounds **4** and **5**, were found to be insoluble in alkanes and toluene and scarcely soluble (≈ 10^{-5} M) in $CHCl_3$ and CH_2Cl_2. Higher solubility is observed in DMSO or in CH_2Cl_2:THF solvent mixtures. Compound **5** proved to be dramatically less soluble than **4** and therefore, only selected analyses have been performed on this molecule.

Probing of the hydrogen bonding ability of 4

Firstly, we probed the propensity of **4** to aggregate though hydrogen bonds as observed previously for **1**,[45] **2**,[45] and other bis-urea compounds.[46, 49, 51-53] A solution of **4** was prepared in CH_2Cl_2:THF (9:1 ratio), THF was required for solubility (*vide supra*) but its amount was minimized in order to favor hydrogen bonding interactions between bis-urea stickers. However, FT-IR analysis of this solution revealed that most of the urea moieties of **4** are not connected to each other through hydrogen bonds (Fig. S1). UV-Vis absorption and other analyses indicated that aggregation between molecules of **4** actually occurs through Pt-Pt and aromatic interactions under these conditions (*vide infra*). This probably explains the poor ability of **4** to form hydrogen-bonded assemblies. On the contrary, most of the urea functions of **(*S*,*S*)-3** are engaged in hydrogen bonds under similar conditions (Fig. S1). We next tested whether the long rodlike chiral assemblies formed by **(*S*,*S*)-3** could promote co-assembly through hydrogen bonding. FT-IR analysis of a 1:1 mixture of **4** and **(*S*,*S*)-3** contradicts this hypothesis since free N−H groups are mostly present (Fig. S1).

Similar mixtures were subsequently evaluated by CD spectroscopy, a more potent probe for detecting interactions between complementary monomers. Sergeants-and-soldiers type experiments were performed in which **(*S*,*S*)-3** and **4** are the sergeant and the soldier, respectively (Fig. 2).[54-55] The mixture with an excess of **(*S*,*S*)-3** relatively to **4** (green spectrum) showed a CD signal centred at λ= 232 nm which is the

ACCEPTED MANUSCRIPT

fingerprint of the chiral supramolecular assemblies formed by **(*S*,*S*)-3** whereas the two other mixtures (brown and orange spectra) are virtually CD silent.[45] Whatever the mixture, the intensity of the CD signal at

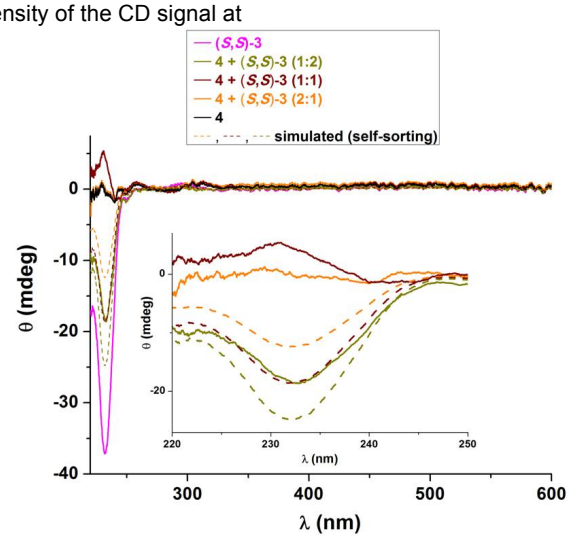

Figure 2 CD spectra of sergeants-and-soldiers type experiments. Spectra of **(*S*,*S*)-3**, of **4** and of their mixtures recorded in CH_2Cl_2:THF (9:1) at T= 263 K (total concentration= 10^{-3} M). Dashed spectra correspond to the weighed sum of the individual spectra, *i.e.* simulated spectra for fully self-sorted assemblies.

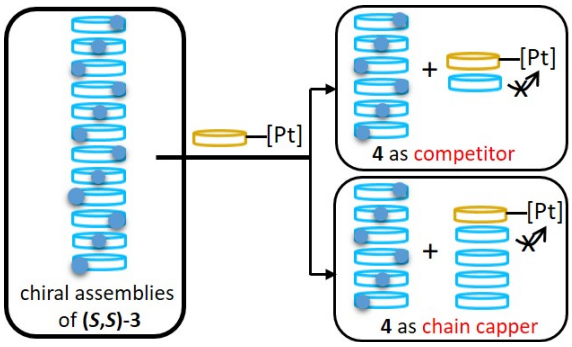

Figure 3 Schematic representation of the co-assembly behaviour between **(*S*,*S*)-3** and **4**. Blue dots represent a monomer in a (*P*) helix. CD analyses indicate that co-assemblies between **3** and **4** lack a preferential handedness and this is represented by the absence of the blue dot. Moreover, the arrow indicates the lack of chirality induction between **(*S*,*S*)-3** and **4** in the co-assemblies. Complex **4** is drawn as a monomer but likely also exists under the form of a head-to-tail dimer as discussed in the text.

232 nm shows no chirality amplification and is even lower than expected for an ideal self-sorting process between the helical assemblies of **(*S*,*S*)-3** and the molecules of **4** (dashed spectra in Fig. 2). Moreover, no CD band is detected at low energy where the "Pt((C^N$^{t\text{-Bu}}^{N}^{t\text{-Bu}}$)" chromophore absorbs (450 nm).

Currently, intensive endeavors are devoted to dissect the nature of the interactions between complementary monomers since it determines the structure of the resulting co-assemblies, notably the monomer sequence and supramolecular polymer length.[56-57] It has recently been demonstrated that a sergeant can adopt different roles depending on its structure, *i.e.* it can intercalate with the soldier to form long hydrogen-bonded assemblies or shorten the assemblies of the soldier by scavenging its monomers or by capping its polymers.[58-59] FT-IR and CD analyses of the mixtures between **(*S*,*S*)-3** and **4** corroborate that cyclometalated Pt complex **4**, *i.e* the soldier, acts as a competitor or chain capper of the helical assemblies formed by **(*S*,*S*)-3.** It is likely that hydrogen bonding of **4** to **(*S*,*S*)-3** prevents further growing of the chain. Induction of chirality is thus precluded by the destabilization of the helical assemblies of **(*S*,*S*)-3** in presence of **4**. The presumed co-assembly behavior between **(*S*,*S*)-3** and **4** is schematically represented in Fig.3.

Aggregation properties of 4 and 5 in DMSO

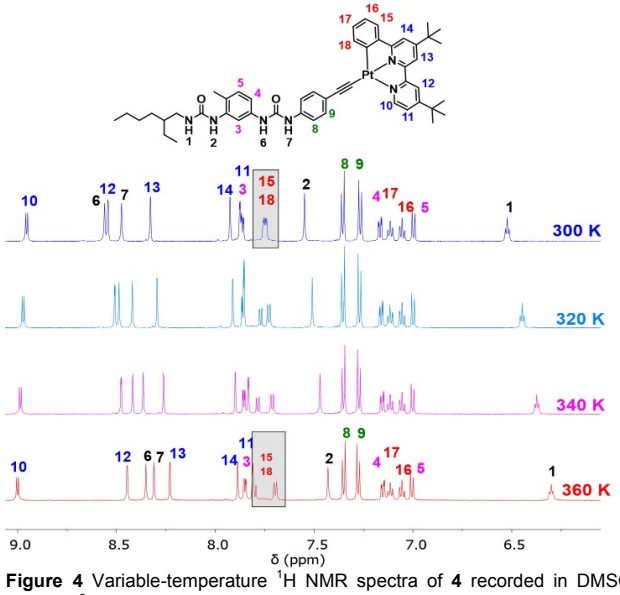

Figure 4 Variable-temperature ^{1}H NMR spectra of **4** recorded in DMSO-d_6 (6.1×10^{-3} M). Zoom on the region corresponding to aromatic C-H and urea N-H.

We next investigated the assembly behavior of **4** and **5** in DMSO, a strong hydrogen bond acceptor that will thus preclude intermolecular hydrogen bonding interactions between Pt-functionalized molecules. Variable-temperature ^{1}H NMR analyses of **4** (Fig. 4) in DMSO-d_6 revealed significant variations in the chemical shifts of aromatic and N−H hydrogens. The largest changes (Table S.1) are experienced by N−H signals that are upfield shifted upon rising the temperature as a probable consequence of the dissociation of the urea−DMSO solvate. On the contrary, aromatic hydrogens are either deshielded or shielded. The more pronounced shifts occur for H10, H12, H13, H15 and H18. For instance, H10 belonging to the pyridyl unit move downfield while H15 and H18, located on the phenyl group of the pincer ligand, overlapped at 300 K but evolved into two doublets of doublets that shifted in opposite directions at higher temperatures (surrounded signals in Fig. 4). These results prompted us to probe the presence of aggregates by measuring the translational diffusion coefficients of **4** and **5** in DMSO-d_6 solution (6.1×10^{-3} M). Thus, ^{1}H DOSY NMR spectra were recorded at different temperatures (Figs. S2 and S3). Analysis of the spectra yielded hydrodynamic radii of 8.2±0.4 Å (resp. 8.5±0.6 Å) and 5.4±0.1 Å (resp. 6.8±0.5 Å) for **4** at 300 K and 340 K (resp. **5**), suggesting a significant decrease in the size of the species at higher temperature. These values are all larger than the hydrodynamic radius calculated for isolated molecules ($R_{monomer}$= 3.6 Å) and dimers (R_{dimer}= 4.5 Å) of **4** in this solvent (see Material and Methods). Considering that aggregates have a spherical shape, aggregation numbers of 12±2 and 13±3 at 300 K, and 3.4±0.2 and 6.5±2, at 340 K are found for Pt complexes **4** and **5**, respectively.[60] These results substantiate the fact that **4** and **5** self-aggregate in DMSO solution, with **5** forming slightly longer oligomers than **4**. The

ACCEPTED MANUSCRIPT

nature of the interactions involved in these aggregates was further probed by UV-Vis absorption and emission analyses.

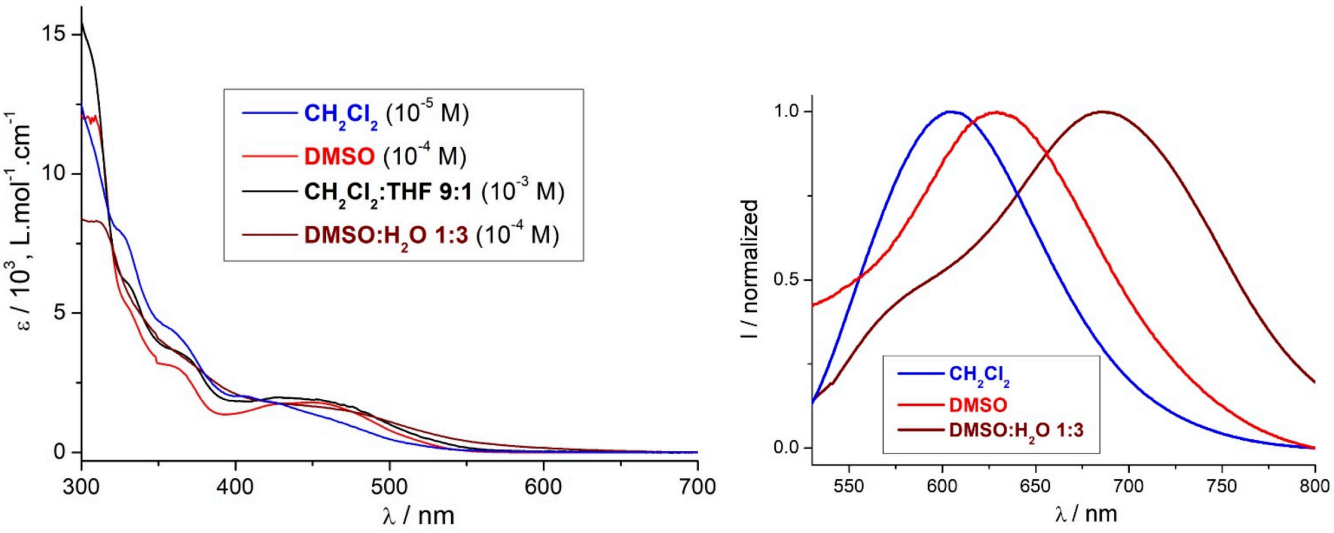

Figure 5 Left: UV-Vis absorption spectra of **4** at 293 K. Right: Normalized emission spectra of **4** at 293 K. λ_{exc}= 450 nm.

Photophysical properties

The UV-visible absorption and emission spectra of **4** and **5** were recorded in various solvents. UV-Vis spectra are shown in Fig. 5 and Fig. S4 for **4** and **5**, respectively. They all display: i) a broad strong absorption band at high energy region (λ<380 nm) which is attributed to ^{1}IL(π-π*) transitions with strong intramolecular charge transfer (ICT) character, as commonly observed for this class of molecules;[20, 47] and ii) a moderately intense low-energy bands with λ_{max} in the range (420-610 nm), assigned to a mixed metal-to-ligand charge transfer ^{1}MLCT (5d)Pt-π*(L) and alkynyl-to-(C^N$^{t\text{-Bu}}^{N}^{t\text{-Bu}}$) ligand to ligand charge transfer (LLCT) [π-alkynyl-π*(L)] transitions with some contribution from ^{1}MMLCT transition as well (*vide infra*).[61-62] The UV-Vis absorption and emission spectra of **4** and **5** are similar (Figs S4 and S6).

In CH_2Cl_2, the low-energy absorption band ends up at *ca.* 500 nm.

Likewise, the emission spectrum (Fig. 5) shows a structureless broad band centred at λ= 596 nm with quantum yield Φ_{em}= 7 x 10^{-3} and an average decay-time of 0.14 μs suggesting a phosphorescent character. With reference to other C^N$^{t\text{-Bu}}^{N}^{t\text{-Bu}}$ platinum complexes reported in the literature, the emission could be tentatively assigned to ^{3}MLCT/^{3}L′LCT transitions.[24, 47] Under similar experimental conditions, complex **5** displays comparable emission characteristics, with Φ_{em}= 8 x 10^{-3} and average decay-time of 0.12 μs. These data are consistent with **4** and **5** being mostly in the monomeric state in CH_2Cl_2 at the concentration under study (10^{-5} M).

In DMSO (10^{-4} M), the low-energy absorption band extends in the red region (up to *ca.* 540 nm). Previous studies of multinuclear complexes featuring the Pt(C^N^N) luminophore indicated that the UV-Vis band at λ_{Abs}> 450 nm can be in part assigned to a ^{1}MMLCT transition.[61-62] The emission band in DMSO is also bathochromically shifted (λ_{em}= 630 nm) relatively to CH_2Cl_2. The broad emission band extends up to 800 nm suggesting some contribution of ^{3}MMLCT is probably taking place.[27] It can thus be inferred that aggregation of **4** (and **5**) in DMSO, as diagnosed above by NMR, occurs through π−π stacking and Pt···Pt interactions. Importantly, the UV-Vis spectrum of **4** in CH_2Cl_2:THF 9:1, *i.e.* the mixed solvent system used to perform the FT-IR and CD analyses mentioned above, is similar to the one recorded in DMSO (Fig. 5). Notably the low-energy band extends up to 540 nm in both spectra. The aggregation of **4** through π−π stacking and Pt···Pt interactions in this solvent mixture likely explains its inability to self-assemble or intercalate with **(*S,S*)-3** through hydrogen bonding (*vide supra*).

Finally, addition of water to DMSO solutions induces even more important bathochromic shifts of the low-energy absorption band and of the emission band; the latter being now centered at λ≈ 700 nm. Similar changes were observed for **5** except that the red shift of the emission was smaller (Fig. S6). It is well established that the presence of water tends to favor the aggregation of Pt alkynyl complexes through π−π stacking and Pt···Pt interactions.[16] Further information about the molecular structure of these assemblies is provided by computational analyses.

Theoretical results

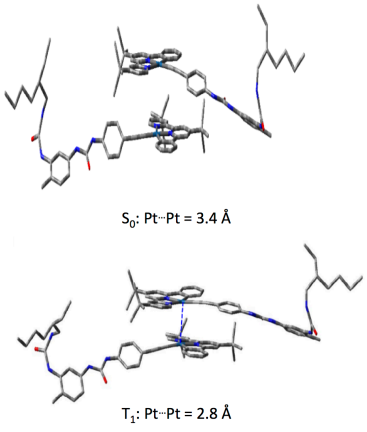

ACCEPTED MANUSCRIPT

Figure 6 PBE1PBE-GD3BJ/Lanl2dzp optimized ground-state (S_0) and lowest triplet excited-state (T_1) geometries with Pt···Pt distances of the *anti*-dimer in DMSO. Hydrogen atoms are omitted for clarity

The ground (S_0) and the lowest triplet excited states (T_1) geometries of **4** were optimized at the DFT PBE1PBE-GD3BJ/Lanl2dzp level of theory in DMSO using the PCM model (see Material and methods). Then, the dimer structure of the complex was built using the ground state optimized geometries. As the dipole moment of the complex is large (18.2 D in DMSO), the *anti* stacking (head-to-tail aggregation) is expected to be the most stable conformation. The absence of specific NOE contacts in the ^{1}H-^{1}H NOESY spectrum of **4** in DMSO-d_6 (Fig. S7), notably between pyridine and arene C-H hydrogens of the (C^N$^{t\text{-Bu}}^{N}^{t\text{-Bu}}$) pincer-type ligand, also goes in favor of a preferred *anti* stacking arrangement, as proposed for other Pt alkynyl complexes in the literature.[6, 16] The geometry of the *anti* dimer was fully optimized in its S_0 and T_1 states at the same level of theory in solution and the obtained structures highlighting the Pt···Pt distances are displayed in Fig 6. These optimized geometries reveal that the Pt···Pt distance is significantly reduced in the T_1 state (2.8 Å) relatively to the S_0 state (3.4 Å).

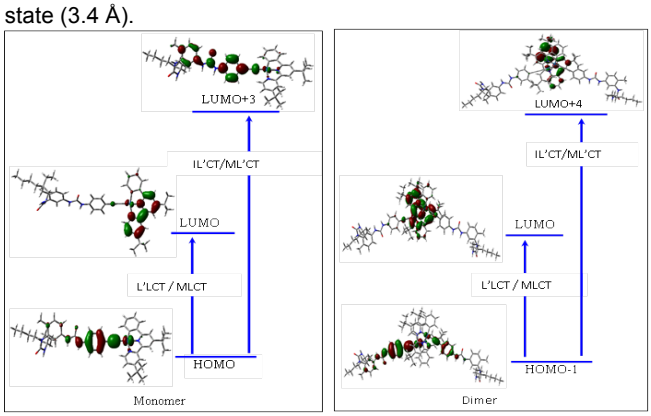

Figure 7 Frontier MO diagrams of the monomer and dimer with main transitions.

The UV-Vis spectra of the monomer and *anti* dimer of **4** have been simulated. The simulated electronic spectra are displayed in Fig. S8 whereas the frontier molecular orbital (MO) diagrams are shown in Fig. 7. The main transitions are described in Table S2. The lowest energy absorption band, calculated for the monomer and the dimer species, corresponds to a HOMO→LUMO (HOMO-1→LUMO for the dimer) transition. This band is assigned to a mixture of L'LCT/MLCT, from the HOMO (HOMO-1) which is delocalized on the platinum and the acetylide−phenyl fragment, with a metallic weight of 13%, to the LUMO localized on the bipyridine moiety of the C^N$^{t\text{-Bu}}^{N}^{t\text{-Bu}}$ pincer ligand. Importantly, this band is red shifted by 37 nm when going from monomer to dimer. A similar bathochromic shift of the lowest energy band is observed for **4** in DMSO:H_2O relatively to CH_2Cl_2 as the result of the aggregation of molecules of **4** through Pt···Pt and π-π interactions in the former solvent.

The theoretical emission energies for the monomer and dimer (Table 1) were calculated as the difference between the energies of the optimized species in the ground (S_0) and lowest triplet excited states (T_1).

Table 1 Calculated emission data for the monomer and dimer.

S_0 (eV)	T_1 (eV)	ΔE (eV, nm)*
Monomer **4**		
-67970.58	-67968.51	2.07, **600**
Dimer $\mathbf{4}_2$		
-135942.55	-135940.86	1.69, **734**

The calculated $T_1 \rightarrow S_0$ emission energy for the monomer translated into a λ_{em} of 600 nm which matches very well the emission band observed for **4** in CH_2Cl_2 (Fig. 5). The calculated λ_{em} for the dimer is close to the one recorded for **4** in DMSO:H_2O mixture (700 nm) which goes in favor of dimers being the predominant species in this solvent mixture. The emission band in DMSO lies in between these two values (λ_{em}= 630 nm) suggesting the presence of both monomers and dimers. It is likely that under diluted conditions, as those of spectroscopic measurements, **4** exists as a mixture of monomer and dimers in pure DMSO and that dimers are the predominant species in DMSO:H_2O mixture. Upon increasing the concentration in pure DMSO, larger aggregates are formed as indicated by the aforementioned DOSY experiments.

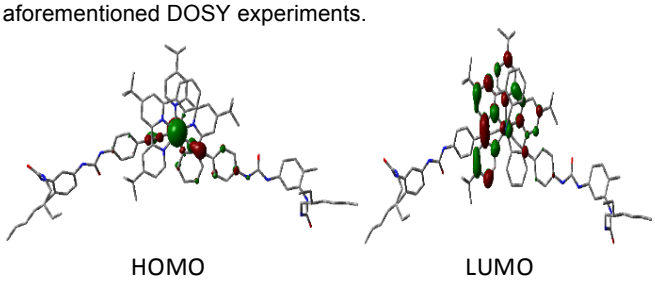

Figure 8 T_1 Frontier MOs of the dimer.

Additional information is gained by comparing the frontier MOs of the dimer in the S_0 and T_1 states. Both LUMOs are localized on the bipyridine moiety of the C^N$^{t\text{-Bu}}^{N}^{t\text{-Bu}}$ pincer ligand. More interestingly, we note that the HOMO of the optimized dimer in the S_0 state is localized on the Pt−acetylide part whilst in the T_1 state it becomes centred on the two platinum atoms (Fig. 8). It can thus be confirmed that the emission band at lower energy observed for the studied Pt complexes originates from metal−metal to ligand charge transfer (^{3}MMLCT), the latter triplet state being characterized by strong Pt···Pt bonding.

Aggregation in solid state and gas phase

Both types of interactions can coexist a priori under solid state or gas-phase conditions. The HR-MS spectrum of **4** showed MS signals corresponding to the monomer $[4 + H]^+$ and more interestingly to the dimer $[\mathbf{4}_2 + 2H]^{2+}$ and the trimer $[\mathbf{4}_3 + 2H]^{2+}$, with experimental isotopic distributions which perfectly matched

ACCEPTED MANUSCRIPT

to the theoretical ones (Fig. S9). This MS analysis further substantiates the ability of the cyclometallated Pt(II) complexes to aggregate into dimers or trimers but the nature of interactions involved in these aggregates remains unknown.

In addition, emission and FT-IR analyses were conducted on complex **4** in the solid state. A structureless broad emission band with λ_{max} at 585 nm extending up to 800 nm is visible (Φ_{em}= 12 x 10^{-3} with average decay-time 0.13 μs).[63] This large band features a triexponential decay emissions at: λ = 580nm, τ = 0.125 μs; at λ = 600 nm, τ = 0.133 μs and at λ = 650 nm, τ = 0.168 μs. The latter indicates that some contribution of ^{3}MMLCT excited states associated with Pt···Pt and π-π aggregation is occurring (Fig. 9a).[62]

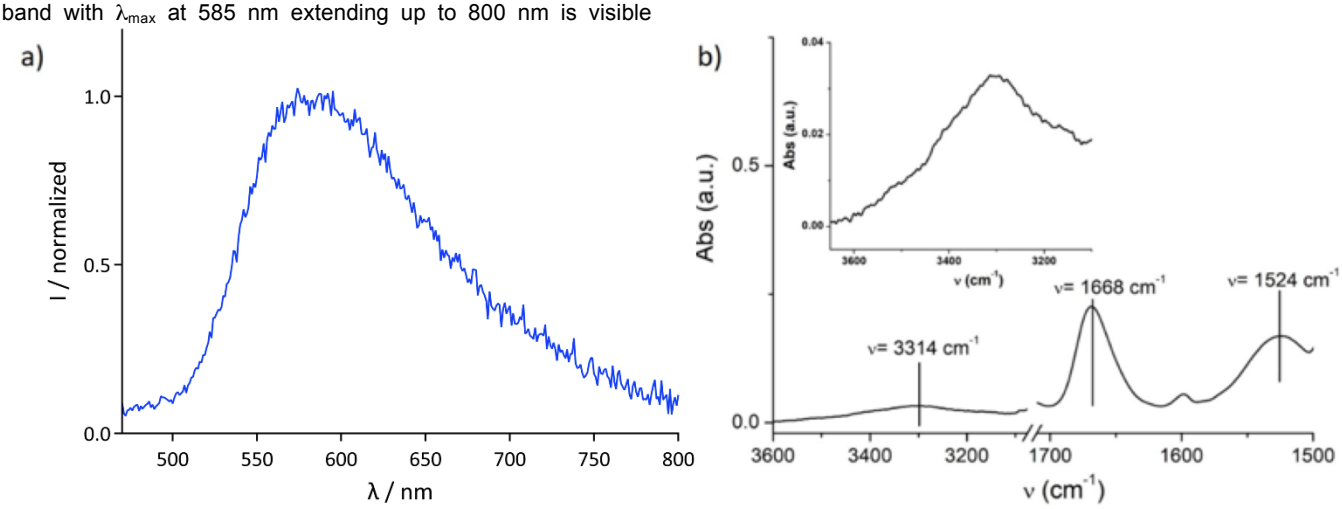

Figure 9 (a) Emission spectrum of **4** recorded in the solid state. (b) FT-IR spectrum of **4** in the solid state (zoom on the N-H and urea C=O regions).

FT-IR bands associated with urea N−H and C=O frequencies are very broad (Fig. 9b) which indicate that the hydrogen bond network is not well organized. Overall, none of the interactions predominate leading to weak interactions between molecules of **4** in the solid state.

Conclusion

We have reported the synthesis of a novel class of neutral cyclometallated platinum complexes [(C^N$^{t\text{-Bu}}^{N}^{t\text{-Bu}}$)Pt-R] (**4−5**) containing a bis-urea alkynyl ligand. The complexes were found to be soluble only in moderately polar or polar solvents despite the presence of *t*-Bu groups on the phenylbipyridine ligand. In CH_2Cl_2:THF, **4** does not self-assemble through hydrogen bonds and acts as a competitor or chain capper of the helical assemblies formed by the complementary enantiopure monomer **(*S*,*S*)-3**, thereby impeding chirality transfer. This is plausibly due to its preferential self-aggregation through π–π stacking and Pt···Pt interactions. Compounds **4** and **5** exhibited phosphorescence in solution at room temperature. VT-NMR, ^{1}H-DOSY NMR, UV-Vis absorption and emission analyses as well as TD-DFT studies demonstrated the ability of these neutral Pt(II) complexes to self-aggregate in DMSO and DMSO:H_2O mixtures. T_1 geometry optimization of the dimer leads to a significant shortening of the Pt···Pt distance compared to the S_0. The HOMO of the optimized dimer in the T_1 state becomes centred on the two platinum atoms, thus, we can conclude that the observed lower emission energy of the studied Pt complexes in DMSO and in DMSO:H_2O originates from metal−metal to ligand charge transfer (^{3}MMLCT). In solid state, only disordered aggregates are present which further supports the competitive rather than cooperative nature of the non-covalent interactions (hydrogen bonding, π–π stacking and Pt···Pt) during aggregation of these functionalized Pt complexes. The possibility of coupling chirality and emission in the same assemblies in order to get circularly polarized light emitters is under investigation in our laboratories.

Experimental Section

Material and methods.

Circular dichroism (CD). CD measurements were performed on a Jasco J-1500 spectrometer equipped with a Peltier thermostated cell holder and Xe laser (lamp XBO 150W/4). Data were recorded at 263 K with the following parameters: 50 nm.min^{-1} sweep rate, 0.05 nm data pitch and 1.0 nm bandwidth. Spectra were corrected for solvent and cell contribution. A quartz cell with a path length of 1.0 mm was used. For all samples, LD contribution was negligible (ΔLD < 0.005 dOD). For all the samples, no linear dichroism effects were present and the shape of the CD signal was independent of the orientation of the quartz slide.

Fourier Transform Infrared (FT-IR) spectroscopy. FT-IR spectra were recorded on a Nicolet iS10 spectrometer using a KBr cell of 2 mm path length and was corrected for air, solvent and cell absorption. FT-IR spectra of the solids were recorded by reflection on a Ge probe (ATR-FTIR).

Photophysics. Absorption spectra of dilute CH_2Cl_2 and DMSO solutions at room temperature (rt) were obtained using a Jasco V-670 UV/Vis spectrophotometer. Molar absorptivity values (ε) were calculated by applying the Lambert-Beer law to low absorbance spectra (A < 1) recorded at successive dilutions. Steady-state photoluminescence spectra were measured in CH_2Cl_2 and DMSO solutions at rt using a Jasco FP-8300 Fluorometer. Corrected emission spectra were obtained on a

ACCEPTED MANUSCRIPT

Fluorolog FL3-221 spectrofluorometer from Horiba Jobin-Yvon. The luminescence quantum yields (Φ_{em}) were determined in solution by using Coumarin 540A in ethanol as a standard at λ_{exc}= 450 nm (Φ_{em}= 0.54) and in solid state by means of an integrating sphere from Horiba Jobin-Yvon. Emission decay curves in solution were obtained by the time-correlated single-photon counting (TCSPC) method with a femtosecond laser excitation composed of a Titanium Sapphire laser (Tsunami, Spectra-Physics) pumped by a doubled Nd:YVO_4 laser (Millennia Xs, Spectra-Physics). Light pulses at 900 nm from the oscillator were selected by an acousto-optic crystal at a repetition rate of 1 MHz, and then doubled at 450 nm by a non-linear crystal. Luminescence photons were detected at 90°, through a polarizer at magic angle and a monochromator, by means of a Hamamatsu MCP R3809U photomultiplier, connected to a SPC-630 TCSPC module from Becker & Hickl. The instrumental response function was recorded before each decay measurement with a full width at half maximum (fwhm) of ~0.7 ns. The fluorescence data were analysed using the Globals software package developed at the Laboratory for Fluorescence Dynamics at the University of Illinois at Urbana-Champaign, which includes reconvolution analysis and global non-linear least-squares minimization method. In solid state, the emission decays were obtained after excitation of the powder sample with a Q-switched nanosecond Nd/YAG laser (λ_{exc}= 450 nm, 8 ns pulse duration, from Continuum Surelite II-10 with OPO) and probed by an Edinburgh Instruments LP920 time-resolved spectrometer. A filter was used to remove the residual excitation light at 450 nm.

Computational details. All calculations have been performed using the Gaussian09-D01 suite of programs.[64] The geometry optimizations have been performed employing the PBE1PBE functional including the Grimme's dispersion correction with Becke-Johnson damping (GD3BJ),[65-66] and the Lanl2dz basis set augmented with polarization functions on all atoms, except hydrogen ones. The solvent effects were taken into account by means of the polarizable continuum model (PCM).[67] Theoretical emission energies were calculated as the difference between the energies of the optimized species in the ground (S_0) and lowest triplet excited states (T_1). Drawings of molecular structures and molecular orbitals were done using GaussView[68] program, whereas theoretical absorption spectra were plotted using Swizard.[69] Percentage compositions of molecular orbitals (MOs) were analyzed using the AOMix[70] program. The hydrodynamic radii of the monomer and dimer of **4** have been calculated as indicated in the SI (caption of Figure S3).

NMR spectroscopy. DOSY ^{1}H NMR experiments were recorded on a Bruker Avance I 400 spectrometer (9.4 T) equipped with an observe broadband probe (BBFO) with z-axis gradient coil with maximum gradient strength of 55.4 G.cm^{-1}. All spectra were acquired in 5 mm NMR tubes. Each NMR tube contained 6.1×10^{-3} M of **4** or **5** in DMSO-d_6. All DOSY experiments were performed using stimulated echo and longitudinal eddy delay with bipolar gradients and two spoil gradients (ledbpgp2s). The diffusion time was Δ= 0.05 s. The duration of the magnetic field pulse gradients δ/2 was adjusted to 1500 µs for **4** at 340 K and 2400 µs at 300 K and 1500 µs for **5** at 340 K and 2500 µs at 300 K. The delay for gradient recovery was 0.2 ms and the eddy current delay at 5 ms. For each DOSY-NMR experiment, a series of 16 spectra on 32 K data points were collected. The pulse gradients (g) were incremented from 2 to 98% of the maximum gradient strength in a linear ramp with a total experiment time of 1h22 min (NS 32). The temperature was set and controlled at 300 K or 340 K with an air flow of 270 L.h^{-1} in order to avoid any temperature fluctuations due to sample heating during the magnetic field pulse gradients. After Fourier transformation and baseline correction, the diffusion dimension was processed with the Topspin 2.1 software. Diffusion coefficients, processed with a line broadening of 1 Hz, were calculated by Gaussian fits with Dynamics Center (Bruker software).

VT-^{1}H NMR experiments were recorded on a Bruker Avance III 600 spectrometer (14,1 T) equipped with 5 mm BBFO probe head (1H / 19F/ BB). Analyses were performed between 300 K and 360 K and a spectrum was recorded every 20 K. All spectra were acquired in a 5 mm NMR tube containing 6.1×10^{-3} M of **4**. The ^{1}H NMR spectra were recorded using a pulse sequence for proton (zg30) with a spectral width of 9615 Hz, an acquisition time of 3.4 s and a number of scans of 16. The spectra were analyzed with TOPSPIN 3.6 (Bruker)/MestreNova.

Synthetic methods

Pd/C (ABCR), Hydrazine hydrate (Sigma Aldrich, 50-60% N_2H_4), 4-ethynylaniline (Sigma Aldrich, 97%), 1-nitro-2,4-dimethylbenzene (Sigma Aldrich, 98%), triphosgene (Sigma Aldrich, 98%), Cs_2CO_3 (Sigma Aldrich, 99%) and 3-methylbutylamine (Sigma Aldrich, >98%), were purchased from the indicated suppliers and used as received. Diisopropylethylamine (DIEA) was distilled over CaH_2. DMSO-d_6 (Eurisotop, 99.8 %) and $CDCl_3$ (Eurisotop, 99.8 %) were used as received. **EHUTE**,[45] [PtCl(C^N$^{t\text{-}Bu}^{N}^{t\text{-}Bu}$)],[47] and **(*R*,*R*)-3**[45] were prepared following published procedures. NMR spectra were recorded on a Bruker Avance III 300, or on a Bruker Avance I 400 spectrometer, or Bruker Avance III 600 and calibrated to the residual solvent peak: DMSO-d_6 (^{1}H: 2.50 ppm; ^{13}C: 39.52 ppm) and $CDCl_3$ (^{1}H: 7.26 ppm; ^{13}C: 77.16 ppm). ^{13}C NMR spectrum of **4** was recorded on Bruker Avance III 600 equipped with 5 mm BBFO probe head at 202 MHz using a pulse sequence UDEFT (Uniform Driven Equilibrium Fourier Transform). Peaks are reported with their corresponding multiplicity (br: broad; s: singlet; d: doublet; t: triplet; q: quadruplet; sept: septet; m: multiplet) and integration, and respective *J* coupling constants are given in Hertz. Exact mass measurements (HRMS) were obtained on TQ R30-10 HRMS spectrometer by ESI+ ionization and are reported in *m/z* for the major signal. FT-IR spectra of the solids were recorded by reflection after evaporation of a MeCN solution on a Ge probe (ATR Harrick apparatus) and the peaks were assigned as strong (s), medium (m) or broad (br).

Synthesis of iPentUXE

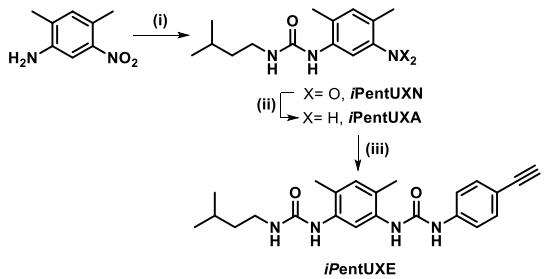

***i*PentUXN:** In an oven-dried Schlenk a solution of 6-nitro-2,4-dimethylaniline (1.50 g, 9.03 mmol) and DIEA (1.70 mL, 9.92

ACCEPTED MANUSCRIPT

mmol) in CH_2Cl_2 (20 mL) was added with a syringe pump (3 mL/h) to a solution of triphosgene (0.94 g, 3.16 mmol) in CH_2Cl_2 (4 mL). The solution was stirred overnight, then 3-methylbutylamine (0.68 g, 9.02 mmol) in CH_2Cl_2 (10 mL) and DIEA (1.70 mL, 9.92 mmol) were added to the solution. The reaction mixture was stirred for 5 hours. The solvent was evaporated under vacuum, and the crude product was extracted with EtOAc (60 mL) and washed successively with HCl 2M, NaOH 1M and brine solutions. The organic phase was dried over $MgSO_4$ and evaporated under vacuum to yield ***i*PentUXN** as a colourless solid (1.39 g, 55%). ^{1}H NMR (300 MHz, DMSO-d_6) δ 8.69 (s, 1H, CH_{Ar}), 7.84 (s, 1H, NH), 7.24 (s, 1H, CH_{Ar}), 6.67 (t, 1H, *J*= 5.6 Hz, NH), 3.12 (q, 2H, *J*= 9.0 Hz, NHCH_2), 2.42 (s, 3H, $C_6H_2CH_3$), 2.23 (s, 3H, $C_6H_2CH_3$), 1.62 (sept, 1H, *J*= 6.8 Hz, CH), 1.34 (q, 2H, *J*= 6.9 Hz, CH_2), 0.92 (d, 6H, *J*= 9.0 Hz, 2×CHCH_3). ^{13}C{^{1}H} NMR (101 MHz, $CDCl_3$) δ 156.6, 147.1, 136.7, 135.1, 134.7, 130.0, 119.8, 39.1, 38.9, 26.0, 22.6, 20.2, 18.3. HRMS (ESI, *m/z*): Calculated for $C_{14}H_{21}N_3O_3H$: $[M+H]^+$: 280.1656, found: 280.1658. FT-IR (ATR, cm^{-1}): 3355 (br), 3290 (br), 2966 (s), 2955 (m), 2879 (m), 1645 (s), 1560 (s), 1533 (s), 1512 (m), 1501 (m), 1337 (m), 1327 (m), 1302 (m).

***i*PentUXA**: ***i*PentUXN** (1.02 g, 3.62 mmol) and Pd/C (5% weight, 50 mg) were suspended in degassed EtOH (50 mL). Hydrazine hydrate (65%, 3.10 mL, 63.5 mmol) was added in one portion and the mixture was refluxed overnight. The reaction was cooled to room temperature and filtered through Celite© pad using AcOEt until no product was left (checked by TLC). The resulting organic phase was washed with H_2O and brine, dried over $MgSO_4$ and the solvent was evaporated under vacuum to yield ***i*PentUXA** (0.61 g, 70%) as a colourless solid. ^{1}H NMR (300 MHz, $CDCl_3$) δ 6.90 (s, 1H, CH_{Ar}), 6.66 (s, 1H, CH_{Ar}), 5.76 (br s, 1H, NH), 4.51 (br s, 1H, NH), 3.58 (br s, 2H, NH_2), 3.22 (q, 2H, *J*= 9.0 Hz, NHCH_2), 2.13 (s, 6H, 2×$C_6H_2CH_3$), 1.62–1.54 (m, 1H, CH), 1.34 (q, 2H, *J*= 7.1 Hz, CH_2), 0.90 (d, 6H, *J*= 9.0 Hz, 2×CHCH_3). ^{13}C{^{1}H} NMR (101 MHz, $CDCl_3$) δ 156.9, 143.5, 134.4, 133.0, 123.1, 120.9, 112.8, 39.3, 38.8, 26.0, 22.6, 17.0, 16.9. HRMS (ESI, *m/z*): Calculated for $C_{14}H_{23}N_3O_1H$: $[M+H]^+$: 250.1914, found: 250.1906. FT-IR (ATR, cm^{-1}): 3410 (br), 3344 (m), 3330 (m), 2964 (m), 2910 (m), 1630 (s), 1562 (s), 1524 (m), 1461 (m), 1447 (m), 1317 (m), 1277 (m), 1248 (m), 1238 (m).

***i*PentUXE** A mixture of 4-ethynylaniline (117 mg, 1.00 mmol) and DIEA (378 µL, 2.20 mmol) in dry THF (3.5 mL) was quickly added with a syringe pump (240 mL/h) to a stirred solution of triphosgene (110 mg, 0.36 mmol) in dry THF (2 mL). After completion of the addition, the solution was stirred for ten additional minutes, then a mixture of ***i*PentUXA** (248 mg, 1.00 mmol) and DIEA (378 µL, 2.20 mmol) in dry THF (10 mL) were added to the solution in one portion. The reaction mixture was stirred for 15 minutes then the solvent was evaporated under vacuum. The crude product was triturated with water (50 mL) and the obtained solid was filtered and recrystallized from MeCN (500 mL). The hot MeCN solution was filtrated yielding 125 mg of a colourless solid. The colourless precipitate obtained at room temperature was also filtered (80 mg). ^{1}H NMR analyses showed that both solids correspond to pure ***i*PentUXE** (205 mg, 52%). ^{1}H NMR (400 MHz, DMSO-d_6) δ 10.06 (br s, 1H, NH_{Ar}), 8.45 (br s, 1H, NH_{Ar}), 8.06 (s, 1H, CH_{Ar}), 7.73 (br s, 1H, NH_{Ar}), 7.50 (d, 2H, *J*= 8.8 Hz, 2×CH_{Ar}), 7.35 (d, 2H, *J*= 8.8 Hz, 2×CH_{Ar}), 6.87 (s, 1H, CH_{Ar}), 6.64 (br, 1H, NH), 4.00 (s, 1H, C≡CH), 3.07 (q, 2H, *J*= 6.8 Hz, NHCH_2), 2.16 (s, 3H, $C_6H_2CH_3$), 2.10 (s, 3H, $C_6H_2CH_3$), 1.68−1.58 (m, 1H, CH), 1.32 (q, 2H, *J*= 7.1 Hz, CH_2), 0.89 (d, 6H, *J*= 6.6 Hz, 2×CHCH_3). ^{13}C{^{1}H} NMR (101 MHz, DMSO-d_6) δ 155.5, 152.7, 141.1, 136.0, 134.7, 132.3, 131.2, 122.4, 122.3, 117.3, 115.5, 113.8, 83.9 (*C*≡CH), 79.0 (C≡*C*H), 37.2, 27.7, 25.1, 22.4, 17.5. HRMS (ESI, *m/z*): Calculated for $C_{23}H_{28}N_4O_2Na$: $[M+Na]^+$: 415.2104, found: 415.2102. FT-IR (ATR, cm^{-1}) : 3315 (br), 2964 (m), 2931 (m), 2912 (m), 1639 (s), 1595 (s), 1545 (s), 1541 (s), 1470 (m), 1309 (m), 1222 (m).

Cyclometallated Pt complex 4

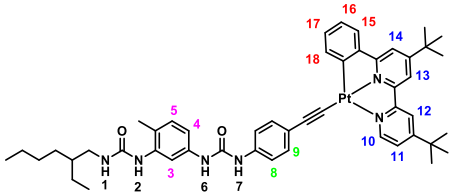

EHUTE[45] (50 mg, 0.12 mmol), [PtCl(C^N$^{t\text{-Bu}}^{N}^{t\text{-Bu}}$)] (69 mg, 0.12 mmol) and Cs_2CO_3 (39 mg, 0.12 mmol) were suspended in MeOH (15 mL) and stirred for 24 h at 50 °C. The suspension was cooled to room temperature and filtered. The precipitate was separated and washed with water (5 mL), MeOH (5 mL) and AcOEt (5 mL), then dried under vacuum to afford **4** as an orange solid (82 mg, 71%). ^{1}H NMR (300 MHz, DMSO-d_6) δ 8.95 (d, 1H, *J*= 5.6 Hz, CH_{Ar}, H10), 8.57 (s, 1H, NH, H6), 8.55 (d, 1H, *J*= 1.7 Hz, CH_{Ar}, H12), 8.48 (s, 1H, NH, H7), 8.33 (d, 1H, *J*= 1.2 Hz, CH_{Ar}, H13), 7.93 (d, 1H, *J*= 1.2 Hz, CH_{Ar}, H14), 7.88 (d, 1H, *J*= 2.1 Hz, CH_{Ar}, H3), 7.86 (dd, 1H, *J*= 5.7 Hz, *J*= 2.0 Hz, H11), 7.76 (dd, 1H, *J*= 3.6 Hz, *J*= 1.1 Hz, H15 or H18), 7.75 (dd, 1H, *J*= 3.6 Hz, *J*= 1.1 Hz, H15 or H18), 7.55 (s, 1H, NH, H2), 7.36 (d, 2H, *J*= 8.7 Hz, 2×CH_{Ar}, H8), 7.27 (d, 2H, *J*= 8.8 Hz, 2×CH_{Ar}, H9), 7.17 (dd, 1H, *J*= 8.1 Hz, *J*= 2.1 Hz, H4), 7.11 (td, 1H, *J*= 7.4 Hz, *J*= 1.3 Hz, H17), 7.05 (td, 1H, *J*= 7.4 Hz, *J*= 1.1 Hz, H16), 6.99 (d, 1H, *J*= 8.5 Hz, H5), 6.52 (t, 1H, *J*= 5.8 Hz, NH, H*1*), 3.11–3.02 (m, 2H, NHCH_2), 2.12 (s, 3H, $C_6H_3CH_3$), 1.46 (s, 9H, $C(CH_3)_3$), 1.43 (s, 9H, $C(CH_3)_3$), 1.41-1.34 (m, 1H, CH), 1.32-1.20 (m, 8H, 4×CH_2), 0.89 (t, 3H, *J*= 5.2 Hz, CH_2CH_3), 0.88 (t, 3H, *J*= 5.5 Hz, CH_2CH_3). ^{13}C{^{1}H} NMR (202 MHz, DMSO-d_6) δ 164.51, 164.26, 163.78, 157.66, 155.45, 154.17, 152.40, 150.58, 147.54, 143.03, 138.52, 137.77, 137.63, 136.97, 131.53, 130.52, 130.10, 125.10, 125.07, 123.34, 122.47, 121.54, 119.66, 117.92, 116.92, 115.97, 111.72, 110.23, 106.69 (C≡C), 104.81 (C≡C), 41.59, 40.06, 35.89, 30.23, 29.99, 28.53, 23.78, 22.55, 17.32, 14.03, 10.90, see attribution by means of ^{1}H–^{13}C HSQC NMR in the SI. HRMS (ESI, *m/z*): Calculated for $C_{49}H_{58}N_6O_2PtH$: $[M+H]^+$: 958.4342, found: 958.4358. FT-IR (ATR, cm^{-1}): 3350 (br), 2960 (m), 2925 (s), 2856 (s), 1745 (s), 1672 (s), 1604 (m), 1533 (s), 1494 (s), 1487 (s), 1446 (s), 1353 (m), 1294 (s), 1242 (s).

Cyclometallated Pt complex 5

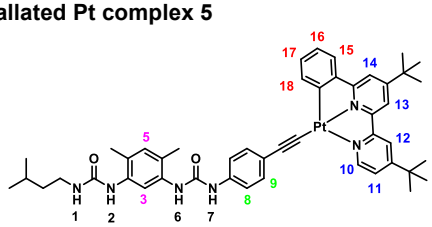

***i*PentUXE** (150 mg, 0.38 mmol), [PtCl(C^N$^{t\text{-Bu}}^{N}^{t\text{-Bu}}$)] (219 mg, 0.38 mmol) and Cs_2CO_3 (124 mg, 0.38 mmol) were suspended in degassed MeOH (20 mL) and stirred for 24 h at 50 °C. The suspension was cooled to room temperature and filtered. The precipitate was separated and washed with water (10 mL),

ACCEPTED MANUSCRIPT

MeOH (10 mL) and AcOEt (10 mL), and then dried under vacuum to give **5** as an orange solid (247 mg, 70%). ^{1}H NMR (400 MHz, DMSO-d_6) δ 9.77 (s, 1H, NH, H6), 8.97 (d, 1H, *J*= 5.7 Hz, CH_{Ar}, H10), 8.56 (s, 1H, CH_{Ar}, H12), 8.41 (s, 1H, NH, H7), 8.35 (s, 1H, H13), 8.05 (s, 1H, H3), 7.93 (s, 1H, CH_{Ar}, H14), 7.91−7.81 (m, 1H, CH_{Ar}, H11), 7.80–7.68 (m, 3H, CH_{Ar}, H15 + H18 + H2), 7.42 (d, 2H, *J*= 8.6 Hz, CH_{Ar}, H8 or H9), 7.25 (d, 2H, *J*= 8.5 Hz, 2H, CH_{Ar}, H8 or H9), 7.15–7.02 (m, 2H, 2×CH_{Ar}, H16 + H17), 6.88 (s, 1H, CH_{Ar}, H5), 6.65 (t, 1H, *J*= 5.2 Hz, NH, H1), 3.10 (q, 2H, *J*= 6.8 Hz, NHCH_2), 2.17 (s, 3H, $C_6H_2CH_3$), 2.11 (s, 3H, $C_6H_2CH_3$), 1.72−1.65 (m, 1H, CH), 1.46 (s, 9H, $C(CH_3)_3$), 1.42 (s, 9H, $C(CH_3)_3$), 1.34 (q, 2H, *J*= 6.8 Hz, CH_2), 0.90 (d, 6H, *J*= 6.6 Hz, 2×CHCH_3). HRMS (ESI, *m/z*): Calculated for $C_{47}H_{54}N_6O_2PtH$: $[M+H]^+$: 930.4029, found: 930.4037. FT-IR (ATR, cm^{-1}): 3336 (br), 2930 (m), 2858 (m), 1747 (s), 1674 (s), 1541 (m), 1495 (m), 1448 (s), 1354 (m), 1298 (m), 1242 (m). Due to solubility limitation ^{13}C NMR data could not be obtained.

Acknowledgements

We would like to thank LabEx MiChem part of French state funds managed by the ANR within the Investissements d'Avenir programme under reference ANR-11-IDEX-0004-02 for support and GENCI-IDRIS and GENCI-CINES for computing time allocation (Grant 2020-2021-080649).

Keywords: Aggregation • Bisurea • Competitor • Luminescence • Pt···Pt interactions • Sergeants-and-soldiers

[1] J. A. G. Williams, in Photochemistry and Photophysics of Coordination Compounds, Vol. 281, **2007**, pp. 205-268.
[2] J. A. G. Williams, Chem. Soc. Rev. **2009**, 38, 1783-1801.
[3] K. M. C. Wong, V. W. W. Yam, Acc. Chem. Res. **2011**, 44, 424-434.
[4] D. Kim, J. L. Bredas, J. Am. Chem. Soc. **2009**, 131, 11371-11380.
[5] V. W. W. Yam, K. M. C. Wong, N. Y. Zhu, J. Am. Chem. Soc. **2002**, 124, 6506-6507.
[6] A. Amar, H. Meghezzi, J. Boixel, H. Le Bozec, V. Guerchais, D. Jacquemin, A. Boucekkine, J. Phys. Chem. A **2014**, 118, 6278-6286.
[7] H. Sesolis, J. Dubarle-Offner, C. K. M. Chan, E. Puig, G. Gontard, P. Winter, A. L. Cooksy, V. W. W. Yam, H. Amouri, Chem. - Eur. J. **2016**, 22, 8032-8037.
[8] H. Sesolis, C. K.-M. Chan, G. Gontard, H. L.-K. Fu, V. W.-W. Yam, H. Amouri, Organometallics **2017**, 36, 4794-4801.
[9] J. Moussa, K. M.-C. Wong, L.-M. Chamoreau, H. Amouri, V. W.-W. Yam, Dalton Trans. **2007**, 3526-3530.
[10] C. A. Strassert, C. H. Chien, M. D. G. Lopez, D. Kourkoulos, D. Hertel, K. Meerholz, L. De Cola, Angew. Chem. Int. Ed. **2011**, 50, 946-950.
[11] C. Po, A. Y. Y. Tam, K. M. C. Wong, V. W. W. Yam, J. Am. Chem. Soc. **2011**, 133, 12136-12143.
[12] S. Y. L. Leung, V. W. W. Yam, Chem. Sci. **2013**, 4, 4228-4234.
[13] C. Po, Z. Ke, A. Y.-Y. Tam, H.-F. Chow, V. W.-W. Yam, Chem. Eur. J. **2013**, 19, 15735-15744.
[14] J. Moussa, K. M.-C. Wong, X. F. Le Goff, M. N. Rager, C. K.-M. Chan, V. W.-W. Yam, H. Amouri, Organometallics **2013**, 32, 4985-4992.
[15] M. Mauro, A. Aliprandi, C. Cebrian, D. Wang, C. Kubel, L. De Cola, Chem. Commun. **2014**, 50, 7269-7272.
[16] H. L.-K. Fu, S. Y.-L. Leung, V. W.-W. Yam, Chem. Commun. **2017**, 53, 11349-11352.
[17] E. Rossi, A. Colombo, C. Dragonetti, D. Roberto, F. Demartin, M. Cocchi, P. Brulatti, V. Fattori, J. A. G. Williams, Chem. Commun. **2012**, 48, 3182-3184.
[18] W. A. Tarran, G. R. Freeman, L. Murphy, A. M. Benham, R. Kataky, J. A. G. Williams, Inorg. Chem. **2014**, 53, 5738-5749.
[19] J. Moussa, K. Haddouche, L.-M. Chamoreau, H. Amouri, J. A. Gareth Williams, Dalton Trans. **2016**, 45, 12644-12648.
[20] S.-W. Lai, M. C.-W. Chan, T.-C. Cheung, S.-M. Peng, C.-M. Che, Inorg. Chem. **1999**, 38, 4046-4055.
[21] O. Colombani, L. Bouteiller, New J. Chem. **2004**, 28, 1373-1382.
[22] M. Y. Yuen, V. A. L. Roy, W. Lu, S. C. F. Kui, G. S. M. Tong, M. H. So, S. S. Y. Chui, M. Muccini, J. Q. Ning, S. J. Xu, C. M. Che, Angew. Chem. Int. Ed. **2008**, 47, 9895-9899.
[23] W. Lu, Y. Chen, V. A. L. Roy, S. S. Y. Chui, C. M. Che, Angew. Chem. Int. Ed. **2009**, 48, 7621-7625.
[24] J. Yi, B. Zhang, P. Shao, Y. Li, W. Sun, J. Phys. Chem. A **2010**, 114, 7055-7062.
[25] P. Savel, C. Latouche, T. Roisnel, H. Akdas-Kilig, A. Boucekkine, J.-L. Fillaut, Dalton Trans. **2013**, 42, 16773-16783.
[26] J.-L. Fillaut, H. Akdas-Kilig, E. Dean, C. Latouche, A. Boucekkine, Inorg. Chem. **2013**, 52, 4890-4897.
[27] J. L. L. Tsai, T. T. Zou, J. Liu, T. F. Chen, A. O. Y. Chan, C. Yang, C. N. Lok, C. M. Che, Chem. Sci. **2015**, 6, 3823-3830.
[28] X. P. Zhang, V. Y. Chang, J. Liu, X. L. Yang, W. Huang, Y. Z. Li, C. H. Li, G. Muller, X. Z. You, Inorg. Chem. **2015**, 54, 143-152.
[29] T. Ikeda, M. Takayama, J. Kumar, T. Kawai, T. Haino, Dalton Trans. **2015**, 44, 13156-13162.
[30] Y. Hu, K. H.-Y. Chan, C. Y.-S. Chung, V. W.-W. Yam, Dalton Trans. **2011**, 40, 12228-12234.
[31] F. K.-W. Hau, H.-S. Lo, V. W.-W. Yam, Chem. Eur. J. **2016**, 22, 3738-3749.
[32] T. Moriuchi, Y. Sakamoto, S. Noguchi, T. Fujiwara, S. Akine, T. Nabeshima, T. Hirao, Dalton Trans. **2012**, 41, 8524-8531.
[33] X.-D. Xu, J. Zhang, L.-J. Chen, X.-L. Zhao, D.-X. Wang, H.-B. Yang, Chem. Eur. J. **2012**, 18, 1659-1667.
[34] Y.-J. Tian, E. W. Meijer, F. Wang, Chem. Commun. **2013**, 49, 9197-9199.
[35] C. Rest, M. J. Mayoral, K. Fucke, J. Schellheimer, V. Stepanenko, G. Fernández, Angew. Chem. Int. Ed. **2014**, 53, 700-705.
[36] Y. Ai, Y. Li, H. L.-K. Fu, A. K.-W. Chan, V. W. W. Yam, Chem. Eur. J. **2019**, 25, 5251-5258.
[37] A. Langenstroer, K. K. Kartha, Y. Dorca, J. Droste, V. Stepanenko, R. Q. Albuquerque, M. R. Hansen, L. Sánchez, G. Fernández, J. Am. Chem. Soc. **2019**, 141, 5192-5200.
[38] K. Y. Kim, J. Kim, C. J. Moon, J. Y. Liu, S. S. Lee, M. Y. Choi, C. L. Feng, J. H. Jung, Angew. Chem. Int. Ed. **2019**, 58, 11709-11714.
[39] G. Moreno-Alcántar, A. Aliprandi, R. Rouquette, L. Pesce, K. Wurst, C. Perego, P. Bruggeller, G. M. Pavan, L. De Cola, Angew. Chem. Int. Ed. **2021**, 60, 5407-5413.
[40] C. Ouyang, Y. G. Li, T. W. Rees, X. X. Liao, J. H. Jia, Y. Chen, X. T. Zhang, L. N. Ji, H. Chao, Angew. Chem. Int. Ed. **2021**, 60, 4150-4157.
[41] S. K.-L. Siu, C. Po, K.-C. Yim, V. K.-M. Au, V. W. W. Yam, Cryst. Eng. Comm. **2015**, 17, 8153-8162.
[42] A. Langenstroer, Y. Dorca, K. K. Kartha, M. J. Mayoral, V. Stepanenko, G. Fernández, L. Sánchez, Macromol. Rapid. Commun. **2018**, 39, 1800191-.
[43] K. K. Kartha, N. K. Allampally, A. T. Politi, D. D. Prabhu, H. Ouchi, R. Q. Albuquerque, S. Yagai, G. Fernández, Chem. Sci. **2019**, 10, 752-760.
[44] O. Kotova, R. Daly, C. M. G. dos Santos, M. Boese, P. E. Kruger, J. J. Boland, T. Gunnlaugsson, Angew. Chem. Int. Ed. **2012**, 51, 7208-7212.
[45] J. Dubarle-Offner, J. Moussa, H. Amouri, B. Jouvelet, L. Bouteiller, M. Raynal, Chem. Eur. J. **2016**, 22, 3985-3990.

ACCEPTED MANUSCRIPT

[46] B. Isare, M. Pensec, M. Raynal, L. Bouteiller, C. R. Chimie **2016**, 19, 148-156.
[47] W. Lu, B.-X. Mi, M. C. W. Chan, Z. Hui, C.-M. Che, N. Zhu, S.-T. Lee, J. Am. Chem. Soc. **2004**, 126, 4958-4971.
[48] F. Ouhib, M. Raynal, B. Jouvelet, B. Isare, L. Bouteiller, Chem. Commun. **2011**, 47, 10683-10685.
[49] B. Isare, G. Pembouong, F. Boué, L. Bouteiller, Langmuir **2012**, 28, 7535-7541.
[50] E. Ressouche, S. Pensec, B. Isare, J. Jestin, L. Bouteiller, Langmuir **2016**, 32, 11664-11671.
[51] V. Simic, L. Bouteiller, M. Jalabert, J. Am. Chem. Soc. **2003**, 125, 13148-13154.
[52] L. Bouteiller, O. Colombani, F. Lortie, P. Terech, J. Am. Chem. Soc. **2005**, 127, 8893-8898.
[53] B. Isare, M. Linares, L. Zargarian, S. Fermandjian, M. Miura, S. Motohashi, N. Vanthuyne, R. Lazzaroni, L. Bouteiller, Chem. Eur. J. **2010**, 16, 173-177.
[54] A. R. A. Palmans, E. W. Meijer, Angew. Chem. Int. Ed. **2007**, 46, 8948-8968.
[55] E. Yashima, N. Ousaka, D. Taura, K. Shimomura, T. Ikai, K. Maeda, Chem. Rev. **2016**, 116, 13752-13990.
[56] B. Adelizzi, N. J. Van Zee, L. N. J. de Windt, A. R. A. Palmans, E. W. Meijer, J. Am. Chem. Soc. **2019**, 141, 6110-6121.
[57] E. Weyandt, M. F. J. Mabesoone, L. N. J. De Windt, E. W. Meijer, A. R. A. Palmans, G. Vantomme, Org. Mater. **2020**, 2, 129-142.
[58] G. Vantomme, G. M. ter Huurne, C. Kulkarni, H. M. M. ten Eikelder, A. J. Markvoort, A. R. A. Palmans, E. W. Meijer, J. Am. Chem. Soc. **2019**, 141, 18278-18285.
[59] M. A. Martinez-Aguirre, Y. Li, N. Vanthuyne, L. Bouteiller, M. Raynal, Angew. Chem. Int. Ed. **2021**, 60, 4183-4191.
[60] L. Herkert, J. Droste, K. K. Kartha, P. A. Korevaar, T. F. A. de Greef, M. R. Hansen, G. Fernandez, Angew. Chem. Int. Ed. **2019**, 58, 11344-11349.
[61] W. Lu, M. C. W. Chan, N. Zhu, C.-M. Che, C. Li, Z. Hui, J. Am. Chem. Soc. **2004**, 126, 7639-7651.
[62] S. W. Lai, T. C. Cheung, M. C. W. Chan, K. K. Cheung, S. M. Peng, C. M. Che, Inorg. Chem. **2000**, 39, 255-262.
[63] A. Sillen, Y. Engelborghs, Photochem. Photobiol. **1998**, 67, 475-486.
[64] M. J. Frisch, G. W. Trucks, H. B. Schlegel, G. E. Scuseria, M. A. Robb, J. R. Cheeseman, G. Scalmani, V. Barone, B. Mennucci, G. A. Petersson, H. Nakatsuji, M. Caricato, X. Li, H. P. Hratchian, A. F. Izmaylov, J. Bloino, G. Zheng, J. L. Sonnenberg, M. Hada, M. Ehara, K. Toyota, R. Fukuda, J. Hasegawa, M. Ishida, T. Nakajima, Y. Honda, O. Kitao, H. Nakai, T. Vreven, J. A. Montgomery Jr., J. E. Peralta, F. Ogliaro, M. J. Bearpark, J. Heyd, E. N. Brothers, K. N. Kudin, V. N. Staroverov, R. Kobayashi, J. Normand, K. Raghavachari, A. P. Rendell, J. C. Burant, S. S. Iyengar, J. Tomasi, M. Cossi, N. Rega, N. J. Millam, M. Klene, J. E. Knox, J. B. Cross, V. Bakken, C. Adamo, J. Jaramillo, R. Gomperts, R. E. Stratmann, O. Yazyev, A. J. Austin, R. Cammi, C. Pomelli, J. W. Ochterski, R. L. Martin, K. Morokuma, V. G. Zakrzewski, G. A. Voth, P. Salvador, J. J. Dannenberg, S. Dapprich, A. D. Daniels, Ö. Farkas, J. B. Foresman, J. V. Ortiz, J. Cioslowski, D. J. Fox, Gaussian, Inc., Wallingford, CT, USA, **2009**.
[65] S. Grimme, J. Antony, S. Ehrlich, H. J. Krieg, Chem. Phys. **2010**, 132, 154104-154123.
[66] S. Grimme, S. Ehrlich, L. J. Goerigk, Comput. Chem. **2011**, 32, 1456-1465.
[67] J. Tomasi, B. Mennucci, R. Cammi, Chem. Rev. **2005**, 105, 2999-3093.
[68] R. D. Dennington, T. A. Keith, J. M. Millam, GaussView, Version5; Semichem Inc.: Shawnee Mission, KS, 2009.
[69] S. I. Gorelsky, Swizard program, revision 4.5, http://www-sg-chem.net/swizard. .
[70] S. I. Gorelsky, AOMix program, http://www.sg-chem.net/AOMix.

ACCEPTED MANUSCRIPT

Entry for the Table of Contents

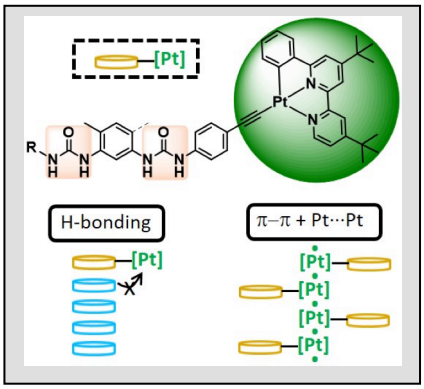

Bis-urea functionalized cyclometalated Pt(II) complex acts as a competitor or chain capper of the helical assemblies form by a complementary enantiopure bisurea (in blue) likely through hydrogen bonding. In more polar media, these complexes exhibit aggregation by means of π–π stacking and Pt···Pt interactions.

ACCEPTED MANUSCRIPT